ACSNANO
www.acsnano.org
ARTICLE

Phenotype Determines Nanoparticle Uptake by Human Macrophages from Liver and Blood

Sonya A. MacParland,[†,‡,⬡] Kim M. Tsoi,[§,∥,⬡] Ben Ouyang,[§] Xue-Zhong Ma,[†] Justin Manuel,[†] Ali Fawaz,[‡] Mario A. Ostrowski,[‡] Benjamin A. Alman,[⊥] Anton Zilman,[#] Warren C.W. Chan,[*,§,¶,△,▼,○] and Ian D. McGilvray[*,†]

[†]Multi Organ Transplant Program, Toronto General Research Institute, University Health Network, 200 Elizabeth Street, Toronto, Ontario, Canada M5G 2C4

[‡]Department of Immunology, University of Toronto, Medical Sciences Building, Room 6271, 1 King's College Circle, Toronto, Ontario, Canada M5S 1A8

[§]Institute of Biomaterials and Biomedical Engineering, University of Toronto, Rosebrugh Building, Room 407, 164 College Street, Toronto, Ontario, Canada M5S 3G9

[∥]Division of Orthopaedic Surgery, University of Toronto, 149 College Street, Toronto, Ontario, Canada M5T 1P5

[⊥]Department of Orthopaedic Surgery, Duke University, Duke University Medical Center, Room 2888, 200 Trent Drive, Durham, North Carolina 27710, United States

[#]Department of Physics, University of Toronto, 60 St. George Street, Toronto, Ontario, Canada M5S 1A7

[¶]Terrence Donnelly Centre for Cellular and Biomolecular Research, University of Toronto, 160 College Street, Room 230, Toronto, Ontario, Canada M5S 3E1

[△]Department of Chemical Engineering, University of Toronto, 200 College Street, Toronto, Ontario, Canada M5S 3E5

[▼]Department of Chemistry, University of Toronto, 80 St. George Street, Toronto, Ontario, Canada M5S 3H6

[○]Department of Material Science and Engineering, University of Toronto, 160 College Street, Room 450, Toronto, Ontario, Canada M5S 3E1

Supporting Information

ABSTRACT: **A significant challenge to delivering therapeutic doses of nanoparticles to targeted disease sites is the fact that most nanoparticles become trapped in the liver. Liver-resident macrophages, or Kupffer cells, are key cells in the hepatic sequestration of nanoparticles. However, the precise role that the macrophage phenotype plays in nanoparticle uptake is unknown. Here, we show that the human macrophage phenotype modulates hard nanoparticle uptake. Using gold nanoparticles, we examined uptake by human monocyte-derived macrophages that had been driven to a "regulatory" M2 phenotype or an "inflammatory" M1 phenotype and found that M2-type macrophages preferentially take up nanoparticles, with a clear hierarchy among the subtypes (M2c > M2 > M2a > M2b > M1). We also found that stimuli such as LPS/IFN-γ rather than with more "regulatory" stimuli such as TGF-β/IL-10 reduce per cell macrophage nanoparticle uptake by an average of 40%. Primary human Kupffer cells were found to display heterogeneous expression of M1 and M2 markers, and Kupffer cells expressing higher levels of M2 markers (CD163) take up significantly more nanoparticles than Kupffer cells expressing lower levels of surface CD163. Our results demonstrate that hepatic inflammatory microenvironments should be considered when studying liver sequestration of nanoparticles, and that modifying the hepatic microenvironment might offer a tool for enhancing or decreasing this sequestration. Our findings also suggest that models examining the nanoparticle/macrophage interaction should include studies with primary tissue macrophages.**

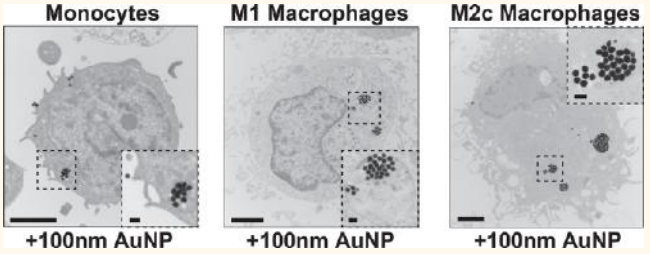

KEYWORDS: *nanoparticle, macrophage, phenotype, phagocytosis, Kupffer cell, cytokine*

Understanding the interactions of nanoparticles with macrophages is key to successfully employing nanotechnology for *in vivo* imaging and therapeutic applications. It has been demonstrated that over 99% of all administered cancer-targeting nanoparticles are sequestered by the organs of the reticuloendothelial system and largely by the macrophage-rich liver. Only 0.7% (median) will accumulate in or interact with solid tumors,[1,2] and many of the administered nanoparticles

Received: September 15, 2016
Accepted: December 31, 2016
Published: December 31, 2016

DOI: 10.1021/acsnano.6b06245
ACS Nano 2017, 11, 2428–2443

will be taken up by macrophages, which are cells of the innate immune system. This low delivery efficiency negatively affects the medical utility and translation of nanomedicines. Thus, it is important to probe and understand the interactions of nanoparticles with monocytes and macrophages.[3]

Macrophages reside in every solid organ.[4] Tissue-resident macrophages are likely derived from circulating monocytes[5,6] and are functionally diverse, playing important roles in tissue homeostasis, repair, and response to foreign pathogens. Macrophages tend to adapt to their tissue location, and their biological function is related to their location within the tissue architecture. Interactions of these cells with nanoparticles are both tissue- and cell-state-specific. This fact complicates the study of nanoparticle/macrophage interactions because it is difficult to obtain fresh human tissue specimens for study. As a result, there has been limited study of nanoparticle uptake by human liver macrophages (Kupffer cells), and it is not known whether animal or human surrogates (such as monocyte-derived macrophages) adequately reflect how human Kupffer cells interact with nanomaterials. Most studies, to date, have focused on understanding how particle design affects cellular uptake, kinetics, and exocytosis. For example, Simmet and co-workers showed that macrophage uptake of polystyrene nanoparticles varies based on the serum proteins that opsonize the particles;[7] Thrall and colleagues demonstrated that uptake of silica and superparamagnetic iron oxide nanoparticles leads to altered macrophage activation in response to lipopolysaccharide (LPS) stimulation.[8] However, the polarization of phagocytic cells may be an important factor in determining the uptake and biological impact of nanoparticles, and this cellular parameter has not yet been fully examined.

One key characteristic of macrophages is their functional plasticity, particularly in the way that their responses change based on the inflammatory microenvironment. They can be subdivided into classically ("M1") and alternatively ("M2") activated categories.[9] "M1" macrophages are thought to be pro-inflammatory, whereas "M2" macrophages are more immunoregulatory in nature.[4] M1 macrophages express increased cell surface major histocompatibility complex class II molecules and, in response to pro-inflammatory stimuli such as endotoxin, generate reactive oxygen species and tumor necrosis factor α (TNF-α). In contrast, M2 macrophages express increased cell surface scavenger receptors and produce high amounts of IL-10.[10] M1 and M2 macrophages have been implicated in different disease processes. For example, tumor-associated macrophages closely resemble the M2 phenotype and promote neoplastic cell proliferation, angiogenesis, and remodeling of the extracellular matrix,[11] whereas M1 macrophages tend to dominate in progressing atherosclerotic plaques.[12] The M1/M2 classification is evolving, and subtypes of macrophages are not thought to be strictly delineated. However, several definitions of macrophages exist (*e.g.*, M2a, M2b, M2c) based on the ability of various cytokine combinations to induce different functional phenotypes *in vitro*.[13−16]

The role of macrophage polarization in governing nanoparticle interaction remains unclear and is the main focus of the current study. Understanding the patterns of uptake and sequestration of nanoparticles by differently polarized macrophages may be critical to explaining the size, shape, and surface chemistry biodistribution patterns of nanoparticles, as well as the effect of nanoparticles on cellular and organ function. With this in mind, we systematically studied the impact of macrophage polarization on nanoparticle uptake using macrophage phenotypes derived *in vitro* from circulating human monocytes and examined how this uptake alters key macrophage inflammatory functions. *In vivo* macrophage phenotypes are much more complex than *in vitro*-derived polarizations: macrophages driven *in vitro* to an "M1-like" or "M2-like" state will share some but not all features of M1 and M2 cells found *in vivo*.[17,18] We examined the effect of nanoparticles on freshly isolated human Kupffer cells and measured uptake in "M1" and "M2-like" cells. An improved understanding of the interactions of nanoparticles with macrophages may lead to solutions that can eventually overcome the "delivery" problem associated with nanotechnology and/or lead to new therapeutic or diagnostic strategies to treat many diseases.

RESULTS AND DISCUSSION

In order to determine how macrophage polarization modulates nanoparticle uptake, we adopted two approaches. (1) We examined nanoparticle uptake by monocyte-derived macrophages, which were differentially polarized *in vitro* using several cytokine cocktails to express a predominantly "M1" or "M2" surface phenotype. (2) We examined nanoparticle uptake by isolated human liver Kupffer cells, which exhibit heterogeneous surface expression of M1 and M2 markers *in vivo*. In our generation of monocyte-derived macrophages, we polarized the cells across the recognized spectrum of "M1"-like and "M2"-like phenotype. Previous studies have demonstrated preferential uptake by M1-like macrophages,[19] and others have shown the opposite effect.[13,20] However, it is well-recognized that derived macrophages are considerably different from primary tissue macrophages. For this reason, we asked whether the prediction of M1/M2 nanoparticle uptake from derived macrophages held true in primary liver macrophages.

Gold Nanoparticle as Model Nanoparticles. Gold nanoparticles are an ideal model for a number of reasons. For example, they can be reproducibly synthesized in a range of sizes; they can be made fluorescent for flow-cytometry-based analysis, and they are clinically relevant, with at least two gold-based nanoformulations currently in clinical trials.[21] We synthesized gold nanoparticles with core diameters of 15, 60, and 100 nm, then PEGylated them and grafted them to Alexa Fluor 750 dye. The fluorescent labeling enabled us to explore the size and surface-chemistry-dependent interactions with macrophages. The nanoparticles were characterized using standard methodologies (see Figure 1 for full characterization). Nanoparticle dose selection was determined as shown in Figure S1.

Polarization of Human-Derived Macrophages. We first isolated circulating monocytes from healthy human donors and polarized them *in vitro* to six cytokine-derived macrophage subtypes. We used six different cytokine cocktails: MCSF-treated only ("unpolarized", considered neither M1 nor M2),[18] IFN-γ/LPS-treated (M1), and IL4/IL-10-, IL-4/IL-13-, LPS/IL-1β-, and TGF-β/IL-10-treated (M2, M2a, M2b, and M2c, respectively) (Figure 2A).[13−16] In order to confirm the impact of our polarization strategies, we assessed surface expression of a panel of M1 and M2 phenotypic markers and intracellular cytokine production. M1 markers included HLA-DR, CD25, and CD86, and M2 markers included CD163, CD206, and CD209.[22] Surface phenotype and intracellular cytokine production showed that, among the six macrophage polarizations, there was a skewing of the macrophage phenotype either toward an "M1"-like or an "M2"-like phenotype (Figure 2B,C and Figure S2). Specifically, IFN-γ/LPS- and LPS/IL-1β-polarized cells showed upregulated expression of M1 macrophage markers HLA-DR, CD25, and CD86 compared to unpolarized, MCSF-treated cells. IL-4/IL-13-,

DOI: 10.1021/acsnano.6b06245
ACS Nano 2017, 11, 2428−2443

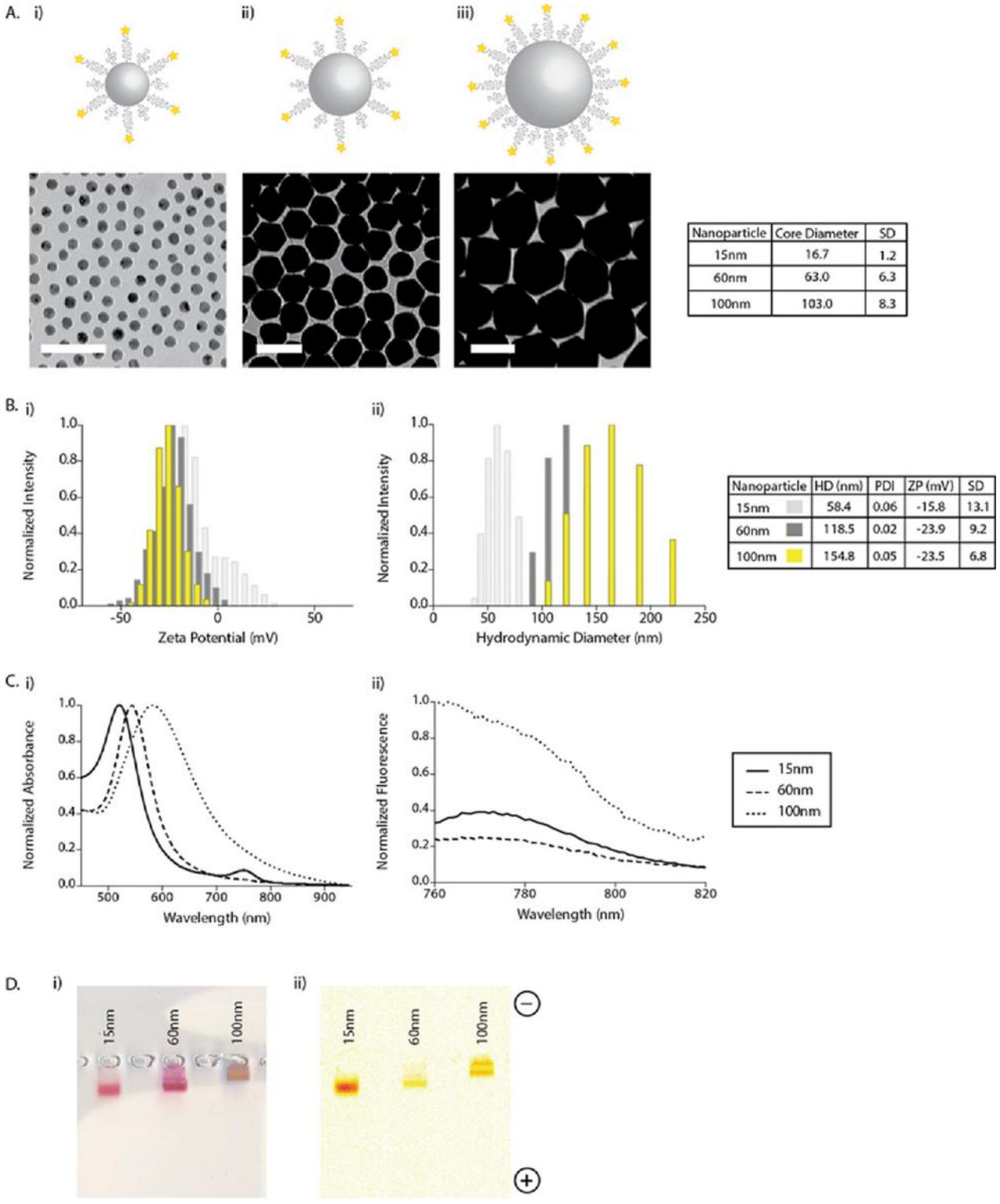

Nanoparticle	Core Diameter	SD
15nm	16.7	1.2
60nm	63.0	6.3
100nm	103.0	8.3

Nanoparticle	HD (nm)	PDI	ZP (mV)	SD
15nm	58.4	0.06	-15.8	13.1
60nm	118.5	0.02	-23.9	9.2
100nm	154.8	0.05	-23.5	6.8

Figure 1. Nanoparticle characterization. (A) Schematic and transmission electron microscopy images of the nanoparticles utilized in this study: 15 nm (i), 60 nm (ii), and 100 nm (iii) gold nanoparticles were grafted with six poly(ethylene glycol) molecules/nm^2 nanoparticle surface area (85% 5 kDa methoxy-PEG-SH and 15% 10 kDa amine-PEG-SH), and subsequently, a 1:1 molar ratio of NHS-Alexa Fluor 750 dye/amine-PEGSH was added to yield fluorescently labeled gold nanoparticles. Electron microscopy images were used to measure nanoparticle core size, and values are included in a table. Scale bar is 100 nm. (B) ζ-Potential (i) and hydrodynamic diameter (ii) of the three nanoparticle sizes with corresponding values included in the table. Hydrodynamic diameter measurements were conducted in water, and ζ-potential measurements were conducted in 1× HEPES buffer (pH 7.15). Abbreviations: hydrodynamic diameter, HD; polydispersity index, PDI; ζ-potential, ZP; standard deviation, SD. (C) Optical properties of the fluorescent gold nanoparticles. Shown are absorbance spectra (i) and fluorescence values (ii) for the three nanoparticle sizes. Fluorescence values were normalized to total nanoparticle surface area. (D) Gel electrophoresis (0.7% agarose, run in 0.5× TBE buffer, 135 mV × 30 min), suggesting that the dye molecules are conjugated to the gold nanoparticles. Shown are bright-field (i) and fluorescence (ii, ex/em = 750/830 nm) images.

DOI: 10.1021/acsnano.6b06245
ACS Nano 2017, 11, 2428−2443

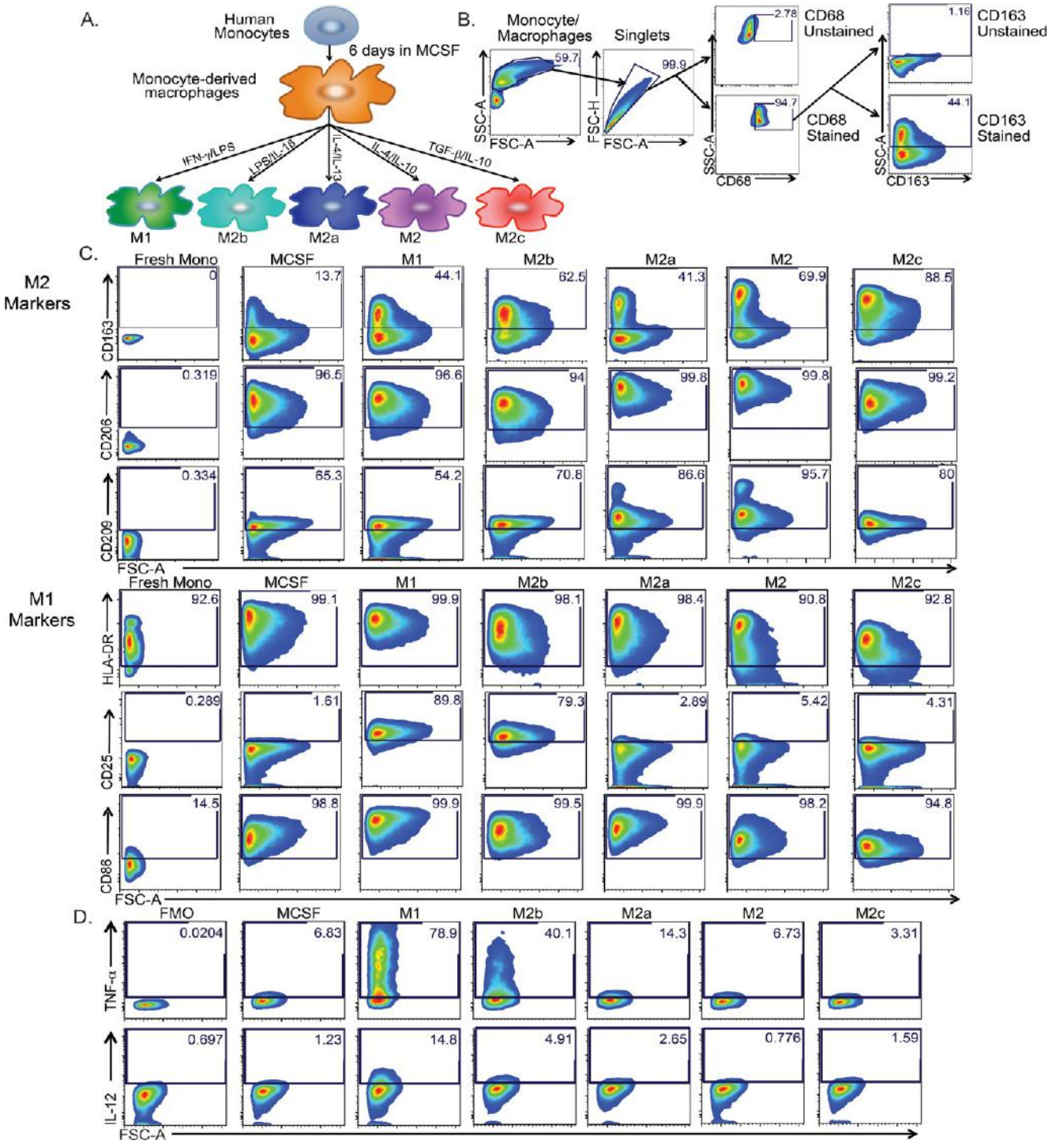

Figure 2. Confirmation of monocyte/macrophage polarization. (A) Monocyte-derived macrophage polarization strategy. MCSF was used to mature purified monocytes to macrophages, and the following cocktails were applied to generate five additional macrophage polarizations: M1, IFN-γ/LPS; M2b, LPS/IL-1β; M2a, IL-4/IL-13; M2, IL4/IL-10; and M2c, TGF-β/IL-10. (B,C) Surface phenotype of each macrophage polarization was determined by flow cytometry, and a total of 20 000 events were collected and analyzed by FACS. Polarized macrophages were stained with CD68 to identify monocytes/macrophages and with anti-human HLA-DR, CD25, and CD86 (M1 surface markers) and anti-human CD163, CD206, and CD209 (M2 surface markers). (B) Gating strategy: Mononuclear cells were identified in SSC-A *vs* FSC-A *via* backgating based on CD68 staining. Singlets were defined as having similar area and height measurements in forward scatter (FSC-A *vs* FSC-H). Macrophages were then identified by CD68+ gating. Gates for surface stains set based on unstained controls. (C) Flow cytometry plots showing expression of surface markers. Gates were set based on background in NP-treated unstained controls. (D) Flow cytometry plots showing secretion of TNF-α and IL-12 after polarizations using the strategy outlined above. Monocyte-derived macrophages were polarized for 18 h, and brefeldin A and monensin were added for the final 6 h of the polarization. Monocytes/macrophages gated as in B. Gating for intracellular cytokine staining was calculated based on fluorescence-minus-one (FMO) controls.

DOI: 10.1021/acsnano.6b06245
ACS Nano 2017, 11, 2428−2443

IL4/IL-10-, and TGF-β/IL-10-polarized cells showed upregulated expression of M2 macrophage markers CD163, CD206, and CD209 (Figure 2C and Figure S2). Cell morphology changed depending on the polarization cocktail, with IFN-γ/LPS-polarized cells (M1-like) being more elongated and IL-4/IL-10- and TGF-β/IL-10-polarized cells (M2-like) having a larger, more rounded morphology (Figure S3). Intracellular cytokine staining revealed that IFN-γ/LPS- and LPS/IL-1β-polarized cells produced TNF-α and IL-12, typical M1 cytokines. The M2 subtype polarizations did not produce detectable amounts of either cytokine (Figure 2D). We were unable to detect the production of IL-6 or IL-10 from any of the subtypes between 18 and 24 h after polarization, and 10−25% of all polarized cells produced IFN-γ, a finding that did not change based on the polarization strategy (Figure S4). Taken together, these data confirm that we were able to successfully generate "M1"-like and "M2"-like macrophage subtypes *in vitro* with the expected surface marker and cytokine expression.

Effect of Monocyte Differentiation on Nanoparticle Uptake. We then studied nanoparticle ingestion by individual macrophage subtypes. For these experiments, freshly isolated monocytes and polarized macrophages were exposed to nanoparticles using a surface-area-normalized dose of 1.06×10^{14} nm^2/well for 4 h in cell culture media supplemented with human serum. Human serum was employed to mimic conditions encountered *in vivo*. Doses were selected based on optimization experiments performed using an immortalized mouse macrophage cell line (see Figure S5A) and M2c-polarized primary human macrophages (see Figure S5B).

We first determined whether nanoparticle size affected uptake by monocytes and polarized macrophages. Nanoparticle uptake was assessed by flow cytometry using two parameters: the percentage of cells that accumulated a detectable amount of nanoparticles (%NP-positive cells) and the mean fluorescence intensity (MFI) of the nanoparticle-positive cells. Regardless of the polarization strategy used, both monocytes and macrophages preferentially took up larger nanoparticles, although macrophages took up considerably more than control monocytes (Figure 3 and Figure S6). In Figure 3Aii,Bi−iv, 0.6 ± 0.5, 21.0 ± 18.9, and 43.5 ± 17.6% of monocytes showed uptake of 15, 60, and 100 nm particles, respectively; IFN-γ/LPS-treated (M1-like) macrophages showed 0.8 ± 0.6, 71.5 ± 17.5, and 87.5 ± 15.3% uptake of 15, 60, and 100 nm particles, respectively; IL-4/IL-10-treated (M2-like) macrophages showed 0.7 ± 0.6, 78.9 ± 17.9, and 94.8 ± 4.1% uptake of 15, 60, and 100 nm particles, respectively; TGF-β/IL-10-treated (M2c-like) macrophages showed 0.6 ± 0.7, 74.7 ± 15.9, and 96.1 ± 2.8% uptake of 15, 60, and 100 nm particles, respectively. Larger nanoparticles were not only ingested by more cells but they were also ingested more avidly: for all polarizations, the MFI for 100 nm nanoparticles was significantly higher than that for 60 nm nanoparticles (Figure 3Bi−iv). Since flow cytometry measures nanoparticle uptake by detecting the conjugated fluorophore rather than the nanoparticle itself, we confirmed uptake using inductively coupled plasma mass spectrometry (ICP-MS) (Figure S5), transmission electron (TEM), and confocal microscopy. TEM images of TGF-β/IL-10-treated macrophages incubated with the three nanoparticle sizes are shown in Figure 3C. Confocal microscopy images for these same cells exposed to 100 nm nanoparticles were also obtained. Both TEM and confocal microscopy demonstrate clear internalization of nanoparticles (Figure 3D). Our finding of preferential uptake of larger nanoparticles by macrophages is in agreement with other *in vitro* studies[23−27] and correlates with *in vivo* studies[28−30] that demonstrate increased clearance of larger nanoparticles by macrophage-rich organs. However, our data show that this tendency is universal across all macrophage phenotypes: larger nanoparticles are taken up by preference in all macrophage subtypes.

Effect of Macrophage Polarization on Nanoparticle Uptake. Having shown that polarized macrophages take up more nanoparticles than monocytes, we then asked whether there were differences in uptake among the different macrophage subtypes. For this purpose, we held nanoparticle size constant and examined the uptake of 100 nm nanoparticles as these particles showed the most robust uptake. We found that, although roughly the same percentage of cells of subtypes took up the nanoparticles, they did so with different avidity. As is shown in Figure 4A−C, per cell uptake of 100 nm nanoparticles in IL-4/IL-10- and TGF-β /IL-10-polarized macrophages was higher than that in IFN-γ/LPS-polarized macrophages and monocytes. Cumulative data for uptake of 100 nm nanoparticles in six separate experiments showed that there was significantly higher nanoparticle uptake for all macrophage polarizations compared to fresh monocytes and a significant difference in the mean MFI for IFN-γ/LPS-polarized (M1) macrophages compared to TGF-β/IL-10-polarized (M2c) macrophages (Figure 4C and Figure S7A). Cumulative data for the uptake of 60 nm NP uptake in four separate experiments showed that there was a significant difference in the mean MFI for M1 macrophages *versus* M2 macrophages (Figure S7B). These data provide evidence that nanoparticle uptake by macrophages can be modulated by inflammatory states: polarizing with inflammatory stimuli such as LPS/IFN-γ rather than with more "regulatory" stimuli such as TGF-β/IL-10 reduces per cell macrophage 100 nm nanoparticle uptake by an average of 40%. Flow cytometry data were entirely consistent with subsequent TEM analysis (Figure 4D). We also include a series of images for TGF-β/IL-10-polarized macrophages taken 30 min (Figure 4Di), 2 h (Figure 4Dii), and 4 h post-incubation (Figure 4Diii) with the 100 nm nanoparticles compared to fresh monocytes and IFN-γ/LPS-polarized macrophages imaged at 4 h post-nanoparticle incubation (Figure 4Div,v). Together, these data clearly demonstrate that the avidity of nanoparticle ingestion is dependent upon macrophage subtype, with a general hierarchy of M2c > M2 > M2b > M2a > MCSF > M1 > monocytes. Previous studies that do not employ strict polarization strategies for individual subtypes, nor clearly define the cellular phenotypes obtained, have shown both M1 > M2 and M2 > M1 nanoparticle ingestion.[13,19,20] These conflicting results highlight the importance of careful macrophage subtype phenotype definition, as well as the plasticity of the cells *in vitro*: primary tissue-resident cells are critical for confirming *in vitro* results. We then asked the question of whether our findings could be confirmed in different hard nanoparticles. We measured uptake of silica nanoparticles *in vitro* in M2c or M1 polarized human macrophages and found that the patterns of uptake were similar to that of AuNPs. As seen in Figure S7C, M2c macrophages took up significantly more silica NP than M1 macrophages. We next evaluated the kinetics of 15, 60, and 100 nm AuNP uptake by differentially polarized macrophages with a 24 h time-course experiment (2, 4, 8, and 24 h). As seen in Figure S8, we found that the initial uptake of 60 and 100 nm NPs among M2c-polarized macrophages is faster compared to that with M1 macrophages. Early uptake speed appears to be different among macrophages of different subtypes with uptake of both 60 and 100 nm NP by M2c macrophages being faster than that of M1 macrophages. It appears at the later

DOI: 10.1021/acsnano.6b06245
ACS Nano 2017, 11, 2428−2443

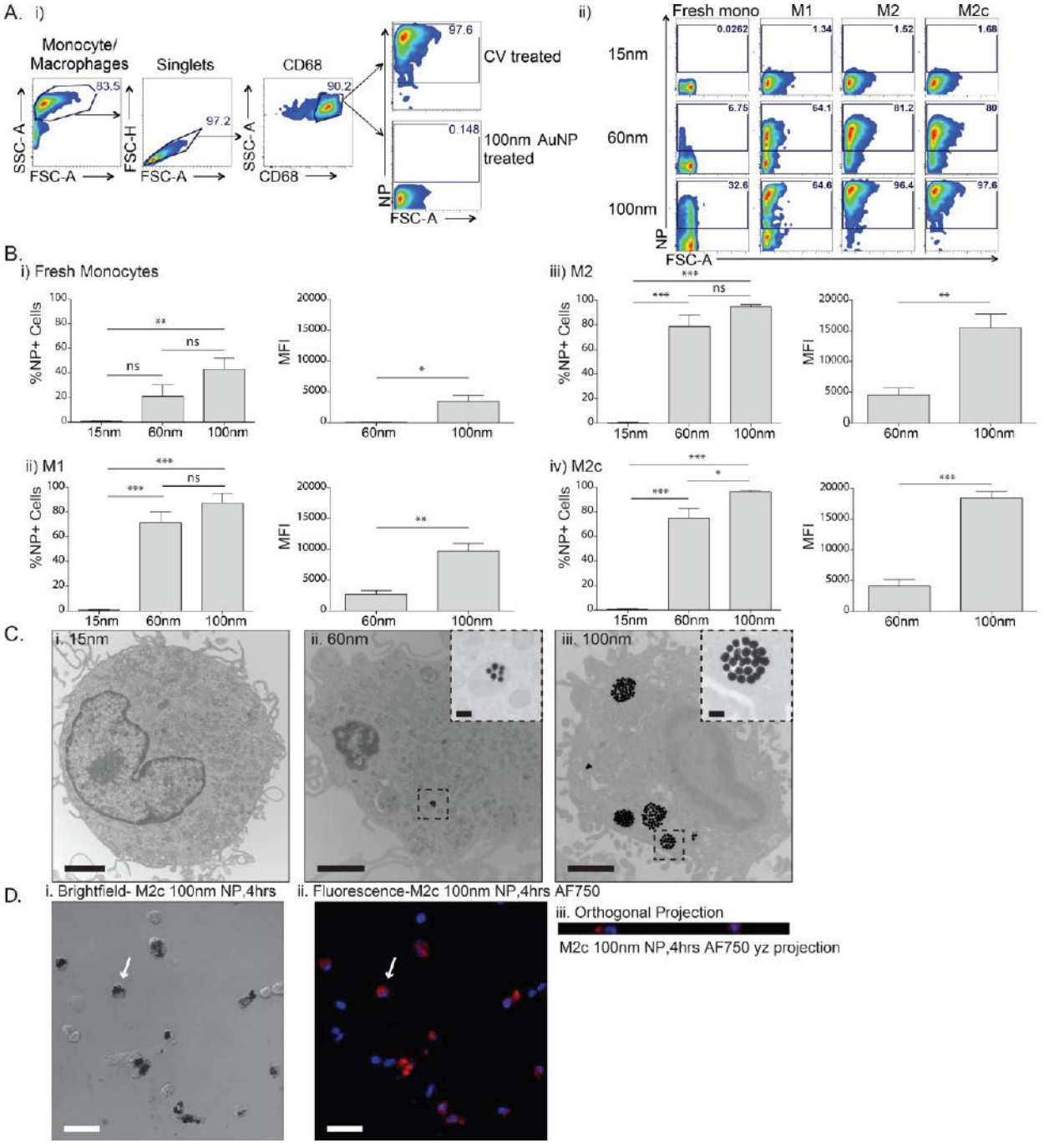

Figure 3. Size-dependent uptake by polarized macrophages. (A) Monocytes and polarized macrophages preferentially take up larger nanoparticles *in vitro*. Monocytes and polarized macrophages were plated and exposed to 15/60/100 nm fluorescent gold nanoparticles for 4 h. Doses were normalized based on total nanoparticle surface area per well. (i) Gating strategy: Mononuclear cells were identified in SSC-A *vs* FSC-A *via* backgating based on CD68 staining. Singlets were defined as having similar area and height measurements in forward scatter (FSC-A *vs* FSC-H). Macrophages were then identified by CD68+ gating. Nanoparticle-positive events gated based on CD68-stained, control-vehicle-treated sample (CV-treated). (ii) Representative flow plots. (B) Percentage and mean fluorescence intensity of each monocyte/macrophage type that is nanoparticle-positive. Error bars are representative of at least four independent experiments ± SEM. Statistical significance was evaluated using an unpaired two-tailed student's *t* test (*$P < 0.001$, **$P < 0.01$, *$P < 0.05$, ns = not significant or $P > 0.05$). (C) Transmission electron microscopy images for M2c macrophages exposed to 15 nm (i), 60 nm (ii), and 100 nm (iii) gold nanoparticles for 4 h. Shown in the main image is nanoparticle location within the cell. The inset includes a high-resolution image of nanoparticles within a membrane-bound intracellular structure. Scale bars are 2 μm in the main image and 200 nm in the inset. (D) Confocal microscopy images for M2c macrophages incubated with 100 nm fluorescent gold nanoparticles for 4 h. These images demonstrate colocalization of the nanoparticles visualized under bright-field illumination (i) with fluorescence from fluorophores grafted to the nanoparticle surface (ii). An orthogonal projection in the *yz* plane of the fluorescence image is shown in (iii). Nucleus is stained with Hoechst 33342 (blue), and nanoparticles appear red. Images were acquired with a 40× PlanApo oil objective (NA 1.3) with the following excitation (ex) and emission (em) wavelengths: nuclei (λ_{ex} = 405 nm; λ_{em} = 450/50 nm), nanoparticles (λ_{ex} = 635 nm; λ_{em} = 770/60 nm). Scale bars are 30 μm.**

DOI: 10.1021/acsnano.6b06245
ACS Nano 2017, 11, 2428−2443

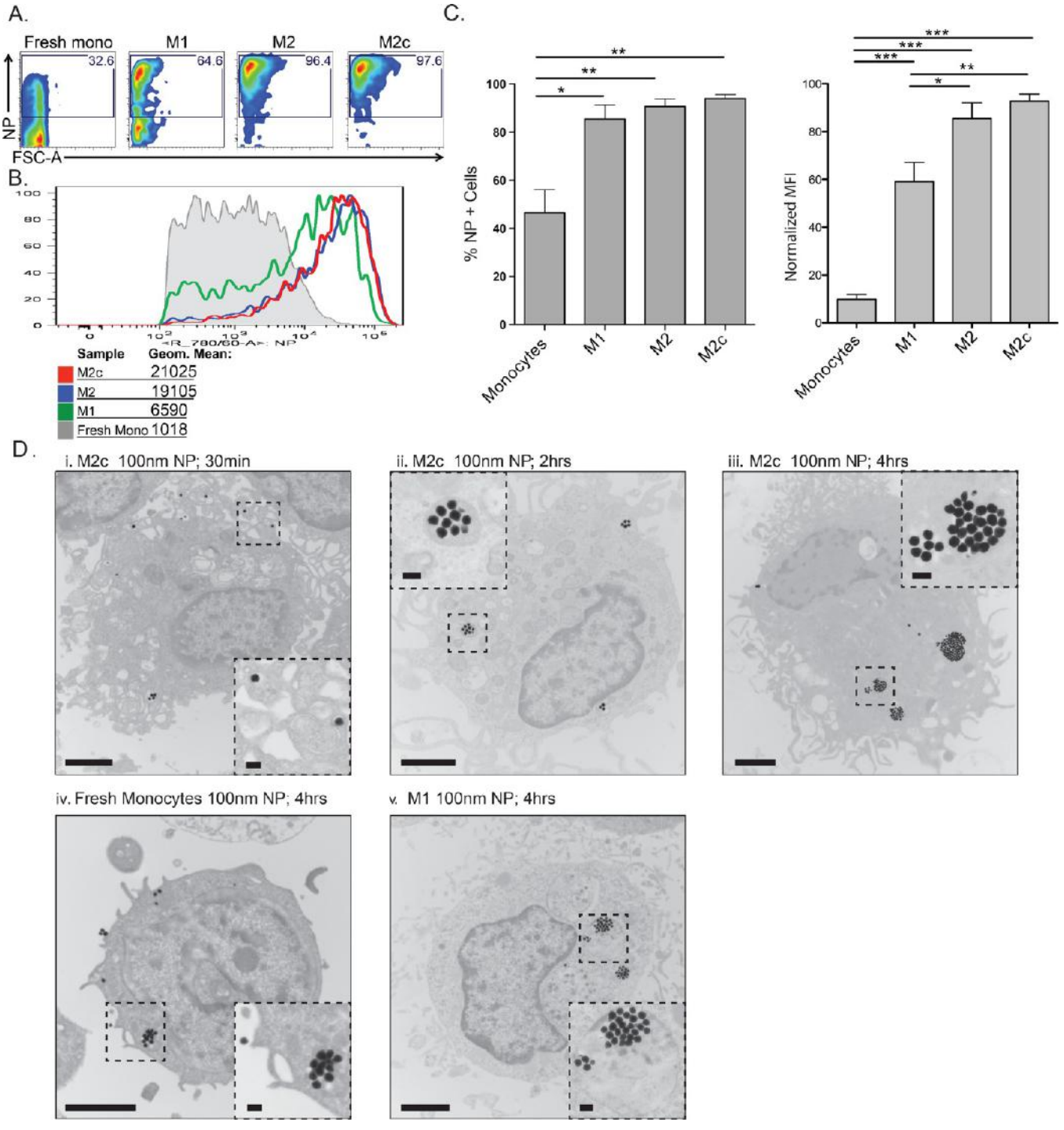

Figure 4. Nanoparticle uptake depends on macrophage polarization. Fresh monocytes (Fresh mono) and polarized macrophages (IFN-γ/LPS, IL4/IL-10, TGF-β/IL-10) were plated and exposed to 100 nm fluorescent gold nanoparticles for 4 h. Dose was normalized based on total nanoparticle surface area per well. (A) Representative flow plots for 100 nm nanoparticles showing the percentage of nanoparticle-positive cells and (B) mean fluorescence intensity for the nanoparticle-positive gate. (C) Percentage and MFI of M1, M2, and M2c macrophages that are nanoparticle-positive following 100 nm AuNP exposure. Error bars are representative of at least six independent experiments ± SEM. MFI for AuNP uptake was normalized for each experiment. Normalized MFI = [MFI for NP uptake/maximum MFI for NP uptake] × 100. Statistical significance was evaluated using an unpaired student's *t* test (*$P < 0.001$, **$P < 0.01$, *$P < 0.05$, ns = not significant or $P > 0.05$). (D) Transmission electron microscopy images for monocytes/macrophages treated with 100 nm fluorescent gold nanoparticles. (i–iii) Time-course images for nanoparticle uptake by M2c macrophages. (i) After a 30 min incubation, individual nanoparticles appear bound to receptors. (ii) After a 2 h incubation, nanoparticles are grouped within membrane-bound intracellular structures. (iii) After a 4 h incubation, more nanoparticles can be seen within membrane-bound intracellular structures. (iii–v) Comparison of 100 nm nanoparticle uptake by M2c macrophages (iii), fresh monocytes (iv), and M1 macrophages (v). Included in (i–v) is one view of nanoparticles in the cell and one high-resolution view focusing on the intracellular nanoparticles. Scale bars are 2 μm in the main image and 200 nm in the inset.**

DOI: 10.1021/acsnano.6b06245
ACS Nano 2017, 11, 2428–2443

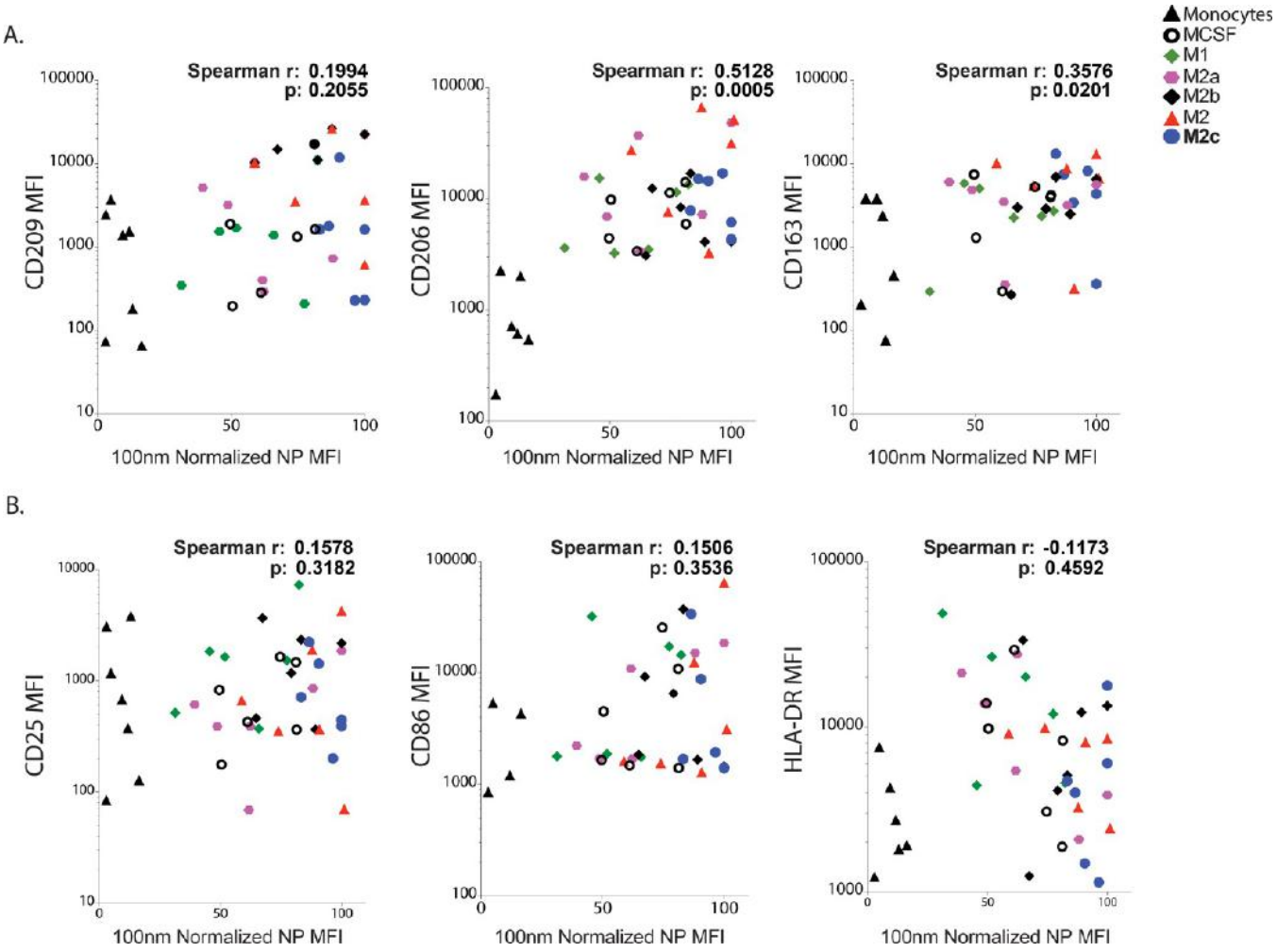

Figure 5. Nanoparticle uptake correlates with expression of M2 markers. Monocytes and polarized macrophages were plated and exposed to 100 nm fluorescent gold nanoparticles or left untreated for 4 h. Dose was normalized based on total nanoparticle surface area per well. Staining was carried out as described in Figure 2. Mean fluorescence intensity for AuNP uptake was normalized for each experiment: 100 nm normalized NP MFI = [MFI for NP uptake/maximum MFI for NP uptake] × 100. (A) M2 markers CD163 and CD206 positively correlate with uptake of 100 nm AuNP. Cumulative plots showing the correlations between CD209, CD206, and CD163 MFI and uptake of 100 nm AuNP. (B) M1 markers do not correlate with uptake of 100 nm AuNP. Cumulative plots showing the correlations between CD25, CD86, and HLA-DR MFI and uptake of 100 nm AuNP. (A,B) Plots show all seven monocyte/macrophage polarizations for six separate experiments. Macrophage classification based on the cytokine cocktail used to derive macrophages. Correlations described using the Spearman's rank correlation coefficient. $P < 0.05$ is considered to be significant.

time point (24 h) that the uptake speed plateaus as macrophages become saturated with nanoparticles, and the differences in NP uptake between M2c and M1 macrophages are no longer significant.

How Does Surface-Marker-Defined Macrophage Phenotype Correlate with Nanoparticle Uptake? As the first step toward defining nanoparticle uptake in primary cells, we then asked whether there were aspects of the surface-marker-defined phenotype that correlate with nanoparticle uptake. Since M2 subtypes ingest nanoparticles more avidly than M1 cells, we hypothesized that M2 surface marker expression would correlate more highly with nanoparticle uptake than M1 surface expression. We found that the expression of typical M2 surface receptors (CD163, CD206) positively correlated with uptake of 100 nm nanoparticles for all phenotypes examined: CD163, Spearman $r = 0.3576$, $p = 0.0201$; CD206, Spearman $r = 0.5128$, $p = 0.0005$ (Figure 5). By contrast, no correlation was found for M1 surface receptors and uptake of 100 nm NP (HLA-DR, CD25, and CD86). This finding that M2 macrophage surface marker expression correlates to NP uptake held true for 60 nm AuNP-treated monocytes and macrophages (Figure S9). These data suggest that surface marker expression may be statistically associated with nanoparticle ingestion; however, using multiple analytical methods, including principle component analysis, surface marker expression was not able to predict nanoparticle uptake. We suspect that a full predictive model for macrophage nanoparticle uptake will require further study with additional surface markers and cellular parameters.

Does Nanoparticle Uptake by Unpolarized Monocytes Shift the Cells' Capacity for Polarization? Monocytes arise from myeloid progenitor cells in the bone marrow, are released into the bloodstream, and migrate to tissue where they differentiate into tissue-specific macrophages such as osteoclasts (bone), Kupffer cells (liver), and microglial cells (central nervous system). For this set of experiments, freshly isolated monocytes were incubated with 100 nm nanoparticles, washed, and then exposed to the established macrophage polarization conditions. We found that nanoparticle uptake prior to monocyte maturation

DOI: 10.1021/acsnano.6b06245
ACS Nano 2017, 11, 2428−2443

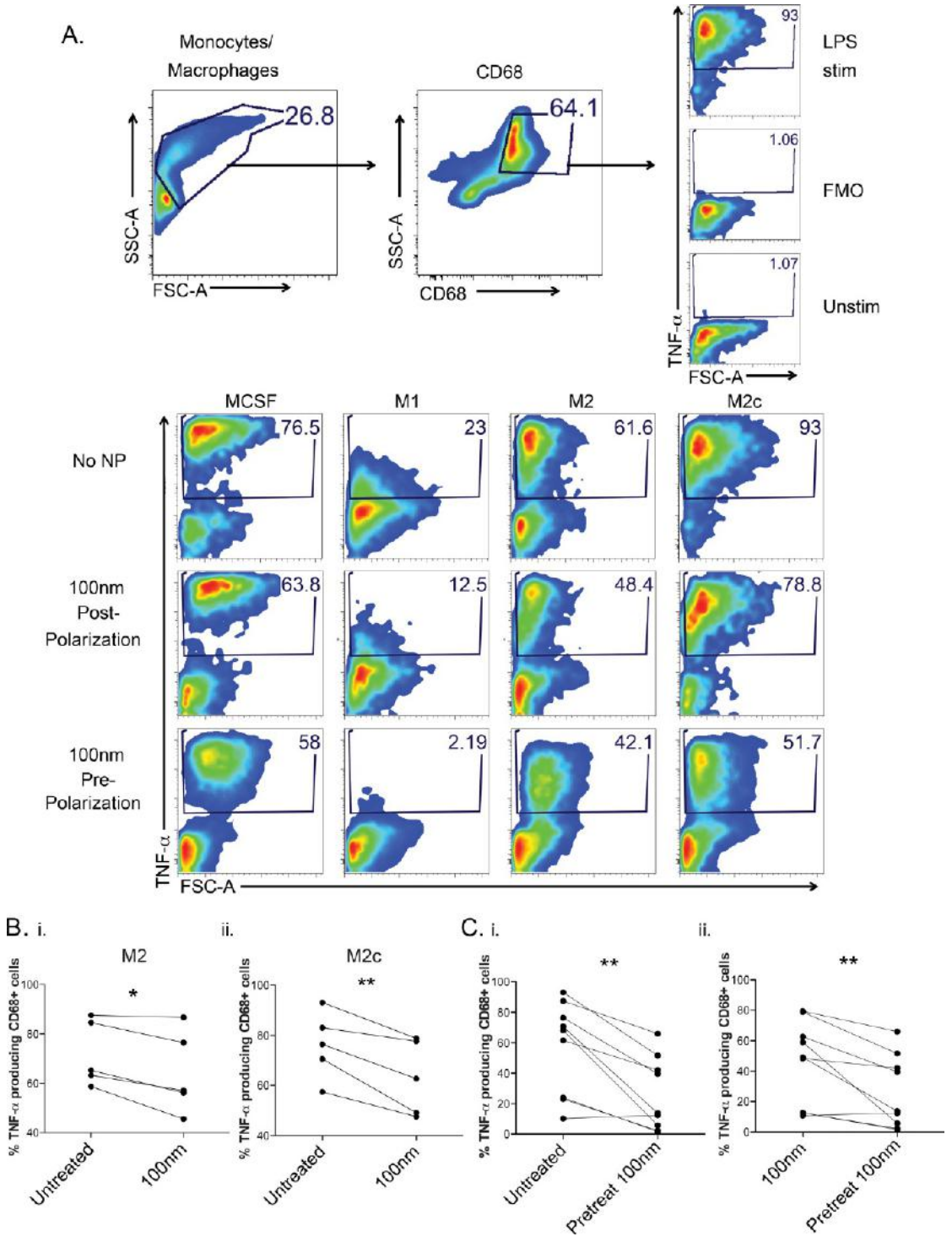

Figure 6. Impact of nanoparticle uptake on macrophage cytokine secretion. (A) Nanoparticle treatment and pretreatment causes macrophages to respond less effectively to LPS stimulation. Purified monocytes were exposed to 100 nm AuNP for 4 h either prior to polarization (100 nm prepolarization) as described in Figure 1, or monocytes were polarized and then exposed to 100 nm AuNP (100 nm postpolarization). All AuNP-treated cells were then further stimulated with 1 μg/mL LPS for 6 h in the presence of brefeldin A and monensin. Gating strategy and representative flow cytometry plots showing secretion of TNF-α after LPS stimulation. Gating for intracellular cytokine staining was calculated based on unstimulated and fluorescence-minus-one (FMO) controls. (B) Percentage of M2- and M2c-polarized macrophages that are TNF-α-positive. Conditions tested were LPS-stimulated macrophages exposed to AuNP postpolarization (100 nm) or not at all (untreated). Data represent five experiments. (C) Cumulative data from three experiments showing LPS-stimulated TNF-α production when comparing NP-treated macrophages to untreated macrophages. (i) Comparison of TNF-α produced by untreated macrophages to monocytes treated with 100 nm AuNP prepolarization (M1, M2, and M2c polarization). (ii) Comparison of TNF-α produced by macrophages treated with 100 nm AuNP postpolarization to monocytes treated with 100 nm AuNP prepolarization (M1, M2, and M2c polarization). Statistical differences in B and C calculated using a paired student *t* test ($P < 0.01$, *$P < 0.05$).**

with MCSF did not prevent monocytes from differentiating into mature macrophages (Figure S10). Thus, nanoparticle uptake *per se* does not seem to alter a monocyte's ability to become a polarized macrophage.

DOI: 10.1021/acsnano.6b06245
ACS Nano 2017, 11, 2428−2443

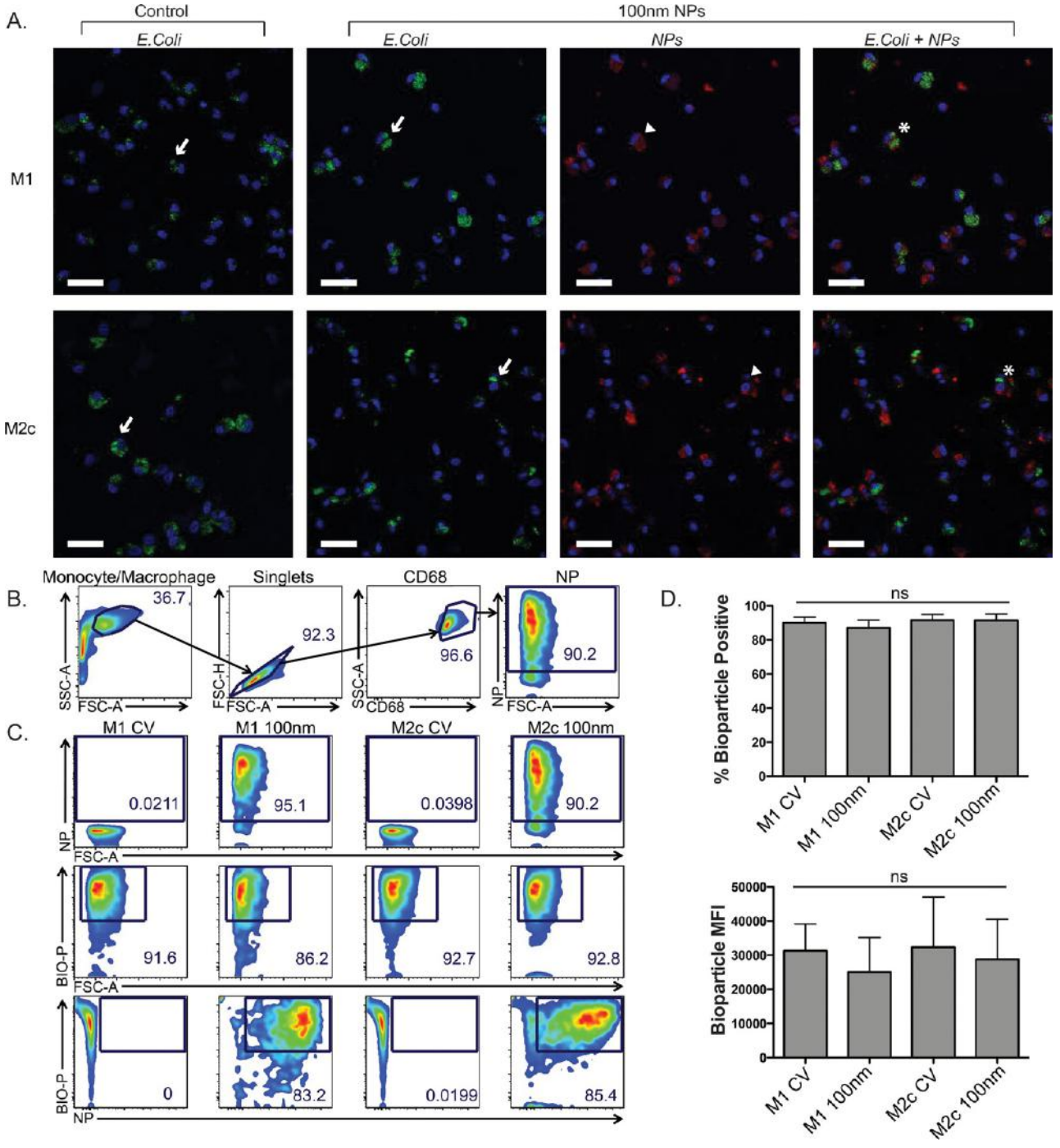

Figure 7. Impact of nanoparticle uptake on phagocytosis. Alexa Fluor 594-conjugated *Escherichia coli* bioparticles (Molecular Probes/Invitrogen) were added to polarized macrophages at a concentration of 10×10^6 bioparticles per well containing 1×10^6 cells (10:1 ratio) and left for 60 min at 37 °C. (A) Confocal microscopy images for the phagocytosis assay performed with IFN-γ/LPS- and TGF-β/IL-10-stimulated macrophages. Shown are results from the phagocytosis assay performed on nanoparticle-untreated cells ("control") or following incubation with 100 nm nanoparticles ("100 nm NPs"). In these images, the nucleus is stained with Hoechst 33342 (blue); phagocytosed *Escherichia coli* appears green, and nanoparticles appear red. Images were acquired with a 40× PlanApo oil objective (NA 1.3) with the following excitation (ex) and emission (em) wavelengths: nuclei (λ_{ex} = 405 nm; λ_{em} = 450/50 nm), Alexa Fluor 594 *Escherichia coli* bioparticles (λ_{ex} = 559 nm; λ_{em} = 620/100 nm), and nanoparticles (λ_{ex} = 635 nm; λ_{em} = 770/60 nm). Scale bars are 30 μm. These images demonstrate similar phagocytosis for nanoparticle untreated and treated polarized macrophages, where examples of cells positive for phagocytosis are marked with an arrow. In addition, for the nanoparticle-treated cells, examples of cells positive for both nanoparticle uptake and phagocytosis are indicated with a triangle and arrow, respectively. The same cell is shown in the overlay annotated with an asterisk. (B) Gating strategy and (C) representative flow cytometry plots showing NP uptake and bioparticle uptake in CD68-stained polarized macrophages. (D) Percentage and MFI of each monocyte/macrophage type that is bioparticle-positive. Error bars are representative of at least three independent experiments ± SEM. Statistical significance was evaluated using an unpaired student's *t* test (ns = not significant or $P > 0.05$).

DOI: 10.1021/acsnano.6b06245
ACS Nano 2017, 11, 2428−2443

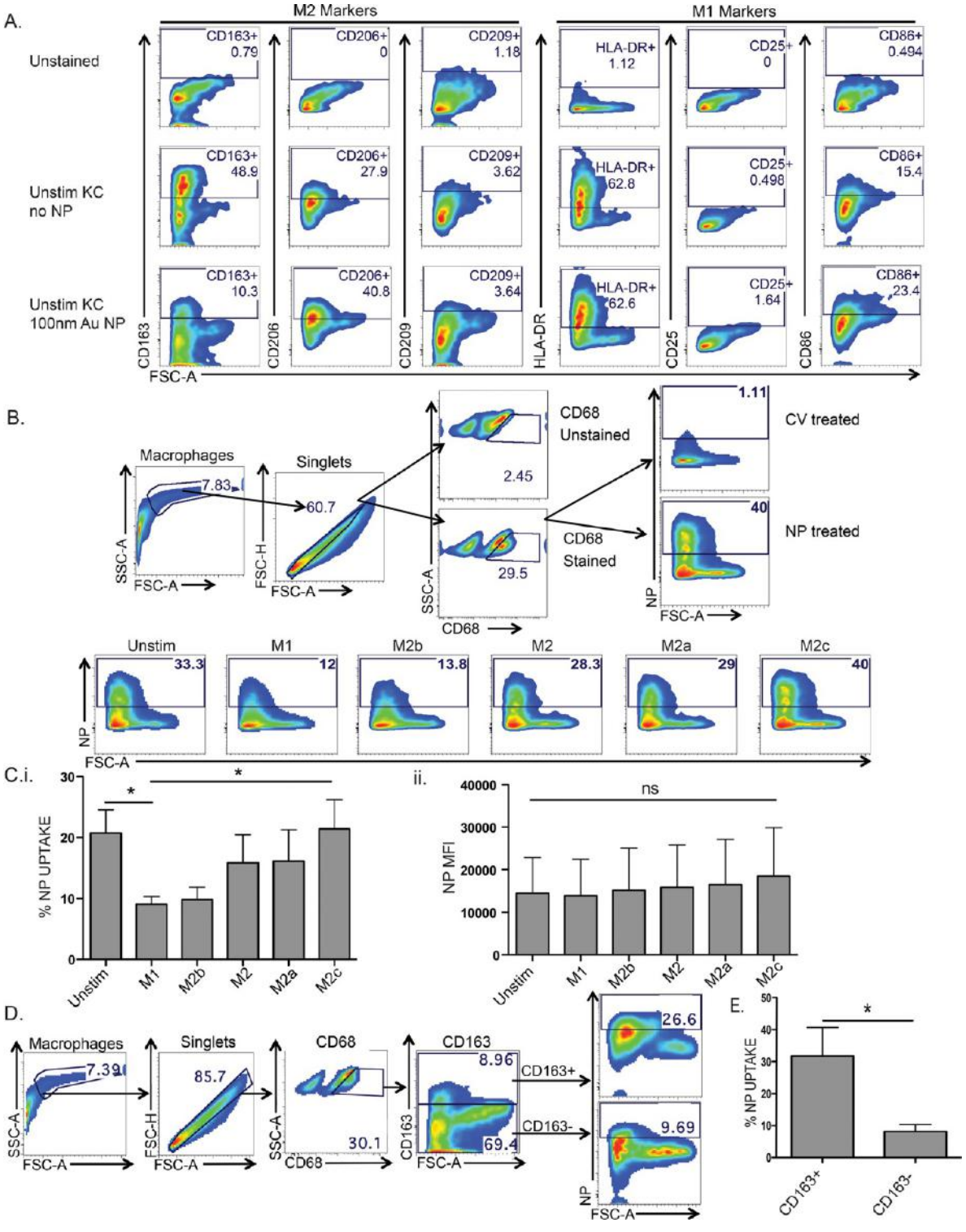

Figure 8. Nanoparticle uptake in primary human Kupffer cells. Primary human Kupffer cells were isolated from total liver homogenate fractionated from caudate lobe of livers used for transplantation. Unpolarized (Unstim KC) and polarized Kupffer cells were plated and exposed to 100 nm fluorescent gold nanoparticles for 4 h. Dose was normalized based on total nanoparticle surface area per well. Cells were then stained with CD68 to identify Kupffer cells and with anti-human HLA-DR, CD25, and CD86 (M1 surface markers) and anti-human CD163, CD206, and CD209 (M2 surface markers). (A) Representative flow plots showing surface phenotype of unstimulated KC with or without exposure to 100 nm AuNP. Cells were gated as shown in Figure 2. (B) Nanoparticle uptake depends on macrophage polarization. Gating strategy and representative flow plots showing NP uptake in Kupffer cells. NP gates set based on a full stained control-vehicle-treated control (CV-treated). (C) Percentage (i) and MFI (ii) of each Kupffer cell polarization that is nanoparticle-positive. (D,E) Unstimulated CD163+ Kupffer cells preferentially take up nanoparticles. (D) Representative flow plots showing 100 nm AuNP uptake after gating on CD163-positive (CD163+) and CD163-negative cells (CD163−). (E) Percentage of CD163+ and CD163− Kupffer cells that are AuNP-positive. Error bars for C and E are representative of at least four independent experiments ± SEM. Statistical significance was evaluated using an unpaired student's *t* test (*$P < 0.05$, ns = not significant or $P > 0.05$).

DOI: 10.1021/acsnano.6b06245
ACS Nano 2017, 11, 2428−2443

Table 1

size	H_2O (mL)	2.5×10^{-2} M gold chloride (mL)	1.5×10^{-2} M sodium citrate (mL)	2.23 nM 15 nm seeds (mL)	2.5×10^{-2} M hydroquinone (mL)
60 nm	96.45	0.984	0.984	1.57	0.984
100 nm	97.66	0.997	0.997	0.34	0.997

Does Nanoparticle Uptake Impact Macrophage Viability, Inflammatory Function, and Phagocytosis of Bacteria? Macrophage viability was measured using Annexin-V and 7-AAD stains, which reflect early and late apoptosis, respectively. We show in Figure S11 that incubation of macrophages with gold nanoparticles even for 7 days did not impact macrophage viability at the doses used. We further demonstrated that NP cytotoxicity over the 4 h incubation period was not responsible for uptake differences of 60 and 100 nm NP among macrophages of different phenotypes (Figure S12). Macrophage inflammatory function was then evaluated *via* cytokine secretion post-LPS challenge and a phagocytosis assay. To investigate inflammatory function, macrophage TNF-α secretion was examined post-nanoparticle uptake and compared to control-vehicle-treated cells. We found that 100 nm nanoparticle uptake both 7 and 1 days prior to LPS stimulation significantly impeded the ability of monocyte-derived macrophages to produce TNF-α (Figure 6A–C). As described previously, the polarization cocktails that included LPS induced a transient refractory state to subsequent LPS stimulation (Figure 6A).[31−33] We observed that nanoparticle treatment pre- or postpolarization led to a significant decrease in TNF-α secretion by *in vitro*-polarized macrophages (Figure 6Bi,ii). The inhibitory effect on TNF-α secretion was most pronounced in TGF-β/IL-10- (M2c) and IL-4/IL-10-polarized (M2) macrophages, which were the macrophages that consistently took up the most nanoparticles. We also observed significantly less TNF-α produced when untreated macrophages were compared to monocytes treated with nanoparticles prior to polarization (Figure 6Ci) and when macrophages that were nanoparticle-treated postpolarization were compared to monocytes pretreated with nanoparticles prior to polarization (Figure 6Cii). Thus, nanoparticle ingestion significantly inhibits the macrophage's secretion of TNF-α in response to an inflammatory challenge, most especially in the M2 and M2c phenotypes, the subtypes that take up more nanoparticles.

We then assessed whether nanoparticle ingestion impedes a macrophage's ability to phagocytose fluorescently tagged *Escherichia coli* bioparticles. As shown in Figure 7A–D, we found that that there was no significant difference in *E. coli* bioparticle uptake in control-vehicle-treated macrophages when compared to that for M1 and M2c macrophages—chosen as the most distinct phenotypes in our data—treated with 100 nm AuNP. These data suggest that nanoparticle internalization does not interfere with the phagocytic function of M1 or M2c macrophages. Taken together, these data suggest that nanoparticle treatment has no impact on macrophage viability or phagocytic ability but does reduce the pro-inflammatory potential of macrophages. Our findings show that certain aspects of macrophage inflammatory function, specifically TNF-α secretion, are altered by nanoparticle uptake, but macrophage cell death and phagocytosis are not impacted, suggesting that this is a selective, nontoxic effect.

Validation of Nanoparticle–Macrophage Interaction with Cells from Deceased Donor Livers for Transplantation. Kupffer cells are particularly relevant for investigation into the macrophage–nanoparticle interaction both because they are key players in the off-target accumulation of injected nanoparticles and because they are the causative cell type in several hepatic disease states.[34,35] Confirmation of monocyte-derived macrophage findings in primary Kupffer cells is a priority due to the fact that macrophages adapt to and are specific for the tissues in which they reside; for example, tissue-specific macrophages express highly individual gene expression signatures.[36,37] As a first step, Kupffer cells isolated from four patients were phenotyped using the same surface markers as in the macrophage polarization experiments. We found that unstimulated Kupffer cells had a phenotype that was distinct from any of our *in vitro*-polarized macrophages, without a clear M1 or M2 phenotype (Figure 8A). This is in agreement with previous murine-based studies, which suggest that Kupffer phenotype is quite complex and can change rapidly in response to change in the intraorgan environment.[38] Given our results associating levels of CD163 and CD206 with nanoparticle ingestion (Figure 5), we would predict that M1-polarized human KC would ingest fewer nanoparticles than unpolarized ones, and that KC stimulated with M2 cytokines would ingest more nanoparticles than KC stimulated by M1 cytokines but not necessarily more than unstimulated KC. Consistent with this hypothesis, we found significantly less AuNP uptake 4 h postexposure in LPS/IFN-γ-polarized Kupffer cells (9.1 ± 2.55%) compared to unstimulated Kupffer cells (20.7 ± 7.64%) or TGF-β/IL-10-polarized Kupffer cells (21.4 ± 9.7%) (Figure 8B,C). Unstimulated and M2-stimulated KC ingest roughly equivalent amounts. These results demonstrate that NP uptake by Kupffer cells can be significantly reduced (by an average of 56%) by inflammatory stimulation with LPS/IFN-γ. Thus, skewing the hepatic cytokine environment may be a strategy to modulate NP accumulation in the liver.

As further evidence of the fact that M2 macrophages are more prone to take up nanoparticles, we looked at nanoparticle uptake in unpolarized primary Kupffer cells and focused on the CD163-positive population (an indication of M2 macrophages) and CD163-negative population (M1 macrophages). In these primary liver cells, we asked the question of whether nanoparticle uptake would be uniform or heterogeneous. In this analysis, we saw heterogeneity in nanoparticle uptake that varied along with CD163 expression, with CD163-positive cells taking up significantly more nanoparticles than CD163-negative cells (Figure 8D,E). These data suggest that surface marker phenotyping may be useful for predicting nanoparticle uptake in primary human tissue macrophages.

CONCLUSION

In summary, our results demonstrate that nanoparticles are preferentially taken up by monocyte-derived macrophages and Kupffer cells that have an M2-like phenotype. Nanoparticle uptake selectively impacts the ability of these macrophages to produce pro-inflammatory cytokines such as TNF-α, without altering cellular viability or phagocytic ability. Primary human liver macrophages are far better than circulating monocytes at nanoparticle ingestion, and polarizing with M1-skewing cytokines significantly inhibits nanoparticle ingestion even in these nanoparticle-avid cells. Thus, hepatic inflammatory microenvironments should be considered when interpreting liver sequestration of nanoparticles, and the manipulation of the

DOI: 10.1021/acsnano.6b06245
ACS Nano 2017, 11, 2428–2443

hepatic microenvironment might offer a tool for increasing or decreasing this sequestration, depending on the goals. Our data suggest that future characterization can lead to predictive tools for primary tissue macrophage nanoparticle ingestion based on surface marker expression—as a means to assess and manipulate potential nanoparticle uptake in individual tissues—and demonstrates that models of the nanoparticle/macrophage interaction must include studies with primary tissue macrophages.

METHODS

Gold Nanoparticle Synthesis and Characterization. In the first stage, 15 nm gold nanoparticles were synthesized by adding trisodium citrate (1 mL, 3%w/v) to 98 mL of double-distilled water in a 250 mL Erlenmeyer flask. The solution was brought to a boil, and gold(III) chloride trihydrate (1 mL, 1% w/v) was rapidly injected under vigorous stirring. The reaction was continued for 7 min, and then the flask was transferred to an ice bath.[39] Five milliliters of the 15 nm gold nanoparticles was set aside for preparation of larger gold nanoparticles. The remainder was concentrated *via* centrifugation after the addition of Tween 20 to a final concentration of 0.05 w/v%. In the second stage, 60 and 100 nm gold nanoparticles were prepared by seed-mediated growth.[40] Specific reagents are outlined in Table 1. Reagents were added to a 250 mL Erlenmeyer flask, in a left-to-right sequence, and the reaction was allowed to proceed overnight at room temperature.

Synthesized nanoparticles were washed three times *via* centrifugation with a citrate buffer (0.1 mg/mL sodium citrate + 0.05 w/v% Tween 20). In order to minimize serum protein adsorption and maximize stability under culture conditions, all three sizes of nanoparticles were PEGylated using a density of 6 PEG molecules/nm^2 nanoparticle surface area (85:15 ratio of 5 kDa sulfhydryl-mPEG/10 kDa sulfhydryl-aminePEG; Laysan Bio MPEG-SH-5000, NH_2PEG-SH-10000). Ligand exchange was carried out at 60 °C for 30 min. PEGylated particles were washed three times using the citrate buffer and then resuspended in a sodium bicarbonate buffer for dye conjugation (0.5 M, pH 8.5). In order to measure gold nanoparticle uptake *via* flow cytometry, Alexa Fluor 750 succinimidyl ester (Invitrogen A-20011) was added in a 1:1 ratio with the amine-PEG. Conjugation took place overnight at 4 °C. Excess dye was then removed *via* two washes in 1× PBST followed by two additional washes in 1× PBS. Gold nanoparticle characterization was carried out *via* standard techniques. Concentration was determined *via* UV−visible spectrophotometry (Shimadzu UV-1601PC). Core and hydrodynamic diameters were measured by transmission electron microscopy (FEI Tecnai 20) and dynamic light scattering (ZetaSizer Nano ZS, Malvern Instruments), respectively. Surface charge was determined *via* ζ-potential measurements (1× HEPES buffer, pH 7.4, ZetaSizer Nano ZS, Malvern Instruments). Successful dye conjugation was confirmed by overlapping bright-field and fluorescent bands on agarose gel electrophoresis (0.7% agarose, 135 V × 30 min; Kodak *in vivo* multispectral imaging system (Carestream Health; 750ex/830em) (Figure 1). The Kodak *in vivo* imager was also employed to determine the per particle fluorescence for each gold nanoparticle size.

Functionalization and Characterization of Fluorescent Silica Nanoparticles. The 100 nm amine-terminated silica nanoparticles were purchased from Nanocomposix (cat# SIAN100), washed twice in 1× HEPES buffer to remove ethanol, and then functionalized with 5 kDa methoxy-poly(ethylene glycol)-succinimidyl valerate (Laysan Bio, cat# PG1-SVA-5k) at a density of 5 PEG/nm^2 nanoparticle surface area. Functionalization was carried out at 37 °C for 4 h. Silica nanoparticles were then rendered fluorescent by adding Alexa Fluor 750 succinimidyl ester (Invitrogen, cat# A-20011) at a density of 1.8 fluorophores/nm^2 nanoparticle surface area. Dye conjugation was carried out at room temperature for 4 h. Nanoparticles were then purified by two washes in autoclaved 1× PBS with 0.05% Tween 20 followed by two washes in autoclaved 1× PBS (centrifugation at 3000*g* × 30 min at 4 °C). Silica nanoparticles were characterized as described for fluorescent gold nanoparticles (see Figure S13).

Isolation of Mononuclear Cells from Human Blood. Whole blood was collected from healthy human volunteers into Vacutainer tubes containing the anticoagulant ACD (BD Vacutainer Systems). Samples were collected with appropriate institutional ethics approval from the University Health Network (REB# 14-7425-AE). Peripheral blood mononuclear cells (PBMC) were isolated from blood by gradient centrifugation in Ficoll-paque Plus (GE Healthcare) and cryopreserved for future use.

***In Vitro* Macrophage Polarizations.** Monocytes were purified from cryopreserved PBMC using the negative-selection-based monocyte isolation kit II (Miltenyi Biotec, Auburn, CA) to a purity of 80% (enriched from 10 to 15%). Cryopreserved monocytes were used for the sake of synchronizing experiments, so that there could be a matched, unpolarized monocyte control for each monocyte-derived macrophage experiment. Affinity-purified monocytes were resuspended in RPMI (Sigma-Aldrich) supplemented with 10% human serum (Sigma-Aldrich) and 1% penicillin/streptomycin (Sigma-Aldrich) and plated on a collagen-coated 12-well plate (Fisher Scientific) at a seeding density of 1 × 10^6 cells/well. A parallel incubation procedure was followed for cells seeded onto coverslips for confocal microscopy. Cells were plated at 37 °C in a humidified incubator with 5% CO_2 in the presence of 100 ng/mL recombinant human MCSF (R&D) for 6 days. Cells were then polarized for an additional 24 h with the following five human cytokine cocktails:[13−16] cocktail 1 (M1), 25 ng/mL IFN-γ (Peprotech) and 1 μg/mL LPS (Sigma); cocktail 2 (M2), 25 ng/mL IL-4 (R&D) and 25 ng/mL IL-10 (Biolegend); cocktail 2 (M1), cocktail 3 (M2a), 25 ng/mL IL-4 and 25 ng/mL IL-13(Biolegend); cocktail 4 (M2b), 100 ng/mL LPS, 25 ng/mL IL-1b (Biolegend); cocktail 5 (M2c), 25 ng/mL TGF-β (Biolegend), 25 ng/mL IL-10 (Biolegend).

Nanoparticle Uptake Experiments. Nanoparticle stock solutions were diluted in autoclaved 1× PBS and added to existing media. Doses for 15, 60, and 100 nm fluorescent gold nanoparticles and 100 nm silica nanoparticles were normalized to total nanoparticle surface area per well. Cells were exposed to 1.06 × 10^{14} nm^2/well of each nanoparticle size for a total of 4 h (rationale for nanoparticle dose selection shown in Figure S1). A time-course experiment for TEM evaluation of uptake was carried out (incubation times of 30 min, 2 h, and 4 h). A time-course experiment measuring 15, 60, and 100 nm AuNP uptake by M1- and M2c-polarized macrophages *via* flow cytometry was carried out (incubation times of 2, 4, 8, and 24 h). At the designated time points, cells were washed with 1× PBS to remove non-adherent nanoparticles, collected with 0.25% trypsin (Life Technologies), and stained for multicolor flow cytometry as described below. Cells used for imaging were washed, stained, fixed, and imaged as described in the Confocal Microscopy section. An Annexin-V/7′AAD stain was employed to demonstrate that 60 and 100 nm NPs were not cytotoxic during a 4 h incubation. Results are reflective of at least three replicates.

Since analysis of nanoparticle uptake by flow cytometry measures uptake of the fluorophore grafted to the nanoparticle surface instead of the nanoparticle itself, control experiments comparing flow cytometry to ICP-MS were conducted. For these studies, we used two approaches: (1) an immortalized murine macrophage cell line (RAW 264.7; ATCC TIB-71) and (2) primary human M2c-polarized macrophages. RAW 264.7 cells or M2c-polarized human macrophages were maintained in culture using DMEM with 10% FBS and 1% penicillin/streptomycin. Cells were seeded into 6-well plates (2 × 10^6 cells/well) and allowed to adhere overnight. Plates were prepared in duplicate, with one analyzed for uptake with flow cytometry and the other analyzed for uptake with ICP-MS. The 15 nm/60 nm/100 nm fluorescent gold nanoparticles were added to the wells in RAW 264.7 cell-seeded plates, and 100 nm NPs were tested in human M2c macrophage-seeded plates due to limited availability of primary human cells. As before, the dose for each size was normalized to total nanoparticle surface area per well. Doses for RAW 264.7 cells ranged between 1.33 × 10^{13} and 4.25 × 10^{14} nm^2 per well in 2-fold increments. The dose for human M2c macrophages ranged from 1.33 × 10^{13} to 1.06 × 10^{14} nm^2 per well. The RAW 264.7 cell plates and the primary human macrophage plates were returned to the incubator for 4 h, after which the wells were washed three times with 1× PBS to remove any adherent nanoparticles, and cells were collected and processed as described for each analytical technique.

Inductively Coupled Plasma Mass Spectrometry. Uptake of 15 nm/60 nm/100 nm fluorescent gold nanoparticles by RAW

DOI: 10.1021/acsnano.6b06245
ACS Nano 2017, 11, 2428−2443

264.7 cells or human M2c macrophages was determined using ICP-MS following described methodology.[41] In this approach, calibration curves were first constructed correlating gold content with nanoparticle number and magnesium content with cell number. Nanoparticle-treated cells were then analyzed for gold and magnesium content to determine the number of nanoparticles per cell for each nanoparticle size and dose. For these experiments, cells were treated with 15 nm/60 nm/100 nm fluorescent gold nanoparticles as described above, washed thoroughly with 1× PBS, and then frozen at −20 °C until the day of ICP-MS analysis. On the day of ICP-MS analysis, samples were digested using a solution of 2.0 v/v% HNO_3 and 0.5 v/v% HCl in nanopure water (60 °C × 1 h). Samples were then diluted to a final volume of 5 mL in nanopure water and analyzed using a NexION ICP-MS (PerkinElmer). Data analysis was performed using Syngistix software (PerkinElmer).

Human Kupffer Cell Experiments. Human liver tissue was obtained from livers procured from deceased donors deemed acceptable for liver transplantation. Samples were collected with appropriate institutional ethics approval from the University Health Network (REB# 14-7425-AE). Donor livers were perfused *in situ* with cold histidine−tryptophan−ketoglutarate (HTK) solution. The donor liver caudate lobe was resected and stored in HTK solution on ice before cell isolation. Single-cell isolation from the resected caudate liver lobe was performed with a "two-step" collagenase procedure.[42] Gas containing 95% O_2/5% CO_2 was used to oxygenate all reagents before perfusing the liver tissue. Two or three irrigation cannulae with olive tips were inserted into the cut surface of the liver lobe. The lobe was then perfused with Hank's balanced salt solution (HBSS) with calcium chloride dehydrate 0.5 μM followed by perfusion with collagenase plus neutral protease (VitaCyte cat# 001-2030 and 003-1000) according to the manufacturers' suggested protocol. Perfusion was carried out in a recirculation manner for 15−20 min or until the liver appeared to break apart slightly under Glisson's capsule. The digested lobe was placed on a crystallizing dish containing 100−200 mL of HBSS with 0.1% human albumin (Sigma). A scalpel was used to cut through the tissue and release cells contained within. Liver homogenate was filtered through nylon mesh followed by a centrifugation at 72*g* for 5 min at 4 °C to remove undigested and connective tissues. The liver cell pellet was washed twice, and cells were resuspended in HBSS with 0.1% human albumin for fractionation. Eight to 12 million viable cells were recovered per gram of tissue yield, as determined by the Beckman ViCell trypan blue system. Caudate lobes were, on average, 15−20 g. Liver cells were centrifuged twice at 50*g* for 3 min (4 °C). The supernatant was centrifuged at 650*g* for 7 min (4 °C). The pellet (containing nonparenchymal cells) was collected, resuspended in 10 mL of HBSS, and layered onto a 50%/25% two-step Percoll gradient in a 50 mL conical tube. The tube was centrifuged at 1800*g* × 15 min (4 °C) with the brake off. Four distinct zones resulted from this step. The supernatant containing mostly debris was discarded. The underlying zone was enriched in endothelial cells and lymphocytes. The subsequent zone was enriched in Kupffer cells and was retrieved. Cell viability and counts were determined using a Vi-CELL cell viability analyzer (Beckman Coulter) and were between 80 and 90% viable. The yield of Kupffer cells was between 2 and 4 × 10^6 cells per gram of tissue. Cells from the Kupffer-cell-enriched fraction were seeded into 12-well plates (1 × 10^6 cells/well) and allowed to adhere for 48 h. Kupffer cells were then incubated with the five M1 or M2 macrophage skewing cocktails as described above and incubated with 15, 60, or 100 nm fluorescent gold nanoparticles at a surface-area-normalized dose of 1.06 × 10^{14} nm^2/well for 4 h.

Multicolor Cytokine Flow Cytometry. Cells were lifted from wells with 0.25% trypsin (Gibco). Fc receptors were blocked with human TruStain FcX (Biolegend) for 10 min at room temperature. Surface phenotype was assessed by incubation of 10^6 cells with fluorophore-conjugated monoclonal antibodies to the following human cell-surface markers: anti-CD68-Alexa Fluor 488 (Biolegend Clone: Y1/82A), anti-CD163-Alexa Fluor 647 (Biolegend Clone: GHI/61), anti-CD25-PE/Dazzle 594 (Biolegend Clone: M-A251), anti-CD209 (DC-SIGN)-PE/Cy7 (Biolegend Clone: 9E9A8), anti-CD14-Pacific Blue (Biolegend Clone: HCD14), anti-CD206-phycoerythrin (Biolegend Clone: 15−2), anti-CD86-PerCP/Cy5.5 (Biolegend Clone: IT2.2), anti-HLA-DR-AF700 (Biolegend Clone: L243). Cells were washed and fixed with BD cytofix/cytoperm fixation buffer (BD Biosciences).

Intracellular Cytokine Staining. Nanoparticle-treated and control-treated monocytes and monocyte-derived macrophages were stimulated for 6 h with 1 μg/mL LPS (Sigma) in the presence of brefeldin A and monensin (1:1000) (BD Biosciences); CD68 surface-labeled cells were fixed and then washed with perm/wash buffer (BD Biosciences), and intracellular cytokine staining was performed using the following anti-human antibodies: anti-IFN-γ-AF700 (BD), anti-TNF-α-PE/Cy7 (Biolegend Clone: MAb11), anti-IL12/23p40-AF647 (Biolegend Clone: C11.5), anti-IL-6-Pacific Blue (Biolegend Clone: MQ2−13A5), anti-IL-10-PerCp/Cy5.5 (Biolegend Clone: JES3-9D7).

Cytotoxicity Staining. Macrophage viability after NP treatment was measured using Annexin-V-Pacific Blue (Biolegend: cat# 640918) and 7-AAD (Biolegend: cat# 420403) stains.

General Gating Strategy. Using forward *versus* side scatter, macrophages were separated from debris by flow cytometric analysis. Singlets were defined as having similar area and height measurements in forward scatter (FSC-A *vs* FSC-H).[43] Gating for intracellular cytokine staining was calculated based on fluorescence-minus-one (FMO) controls. Compensation calculations were performed using BD CompBeads (BD Pharmingen) singly stained with fluorophore-labeled antibodies used in the assay. Events were acquired with a BD LSRFortessa (BD Biosciences). When possible, a total of 20 000 events were collected and analyzed with FlowJo software (Tree Star, Inc.). Data were analyzed, and differences were determined using GraphPad Prism 6 software (GraphPad Software Inc., San Diego, CA).

Phagocytosis Assay. Alexa-594-conjugated *Escherichia coli* bioparticles (Molecular Probes/Invitrogen) were added at a concentration of 10 × 10^6 bioparticles per well (1 × 10^6 cells per well) in M1- or M2c-polarized macrophage cultures that were either treated with 100 nm gold nanoparticles or a control vehicle. M1- and M2c-polarized cells were tested as they showed the lowest and highest uptake of nanoparticles, respectively. Cells were left for 60 min. After being washed, macrophages were stained with anti-human CD68 and double-positive cells were quantified by flow cytometry. The assay was repeated for M1 and M2c cells seeded onto collagen-coated coverslips and analyzed *via* confocal microscopy.

Confocal Microscopy. Macrophages were plated onto collagen-coated coverslips, and assays were performed as detailed above. They were then washed, the nucleus stained with Hoechst 33342 (2 μg/mL; Invitrogen H1399), fixed (4% paraformaldehyde × 10 min), and mounted onto standard microscope slides using ProLong gold antifade mountant (Invitrogen P36930). Cells were imaged using the Olympus FluoView 1000 laser scanning confocal (Olympus America, Melville, NY). Images were acquired with the PlanApo 60× oil objective (NA 1.4). Image processing was performed using ImageJ.

Transmission Electron Microscopy. Fresh monocytes and macrophages were pelleted (1 × 10^6 cells/pellet), fixed in 2% glutaraldehyde in 0.1 M sodium cacodylate buffer, and stored at 4 °C until sectioning. To prepare the grids, cells were rinsed in buffer, fixed in 1% osmium tetroxide in buffer, dehydrated in a graded ethanol series followed by propylene oxide, and embedded in EMBed812 resin. Cells were stained with uranyl acetate and lead citrate. Sections 100 nm thick were cut on an RMC MT6000 ultramicrotome and viewed in an FEI Tecnai 20 TEM. Tissue preparation and imaging were performed at the Advanced Bioimaging Centre, Mount Sinai Hospital, Toronto, Canada.

Statistical Analysis. All data were analyzed using Graphpad Prism version 5.0 software (GraphPad Software, San Diego, CA). For nanoparticle-positive cells, statistical differences were calculated using one-way ANOVA with Bonferroni's multiple comparison post-test. Differences in MFI were calculated using the student's two-tailed *t* test. Differences in cytokine secretion with or without AuNP exposure was calculated using the paired student's *t* test. Correlations were described using the Spearman's rank correlation coefficient.

ASSOCIATED CONTENT

Supporting Information

The Supporting Information is available free of charge on the ACS Publications website at DOI: 10.1021/acsnano.6b06245.

DOI: 10.1021/acsnano.6b06245
ACS Nano 2017, 11, 2428−2443

Additional data showing nanoparticle characterization and the impact of phenotype on nanoparticle uptake (PDF)

AUTHOR INFORMATION

Corresponding Authors

*Tel: +1 416 946-8416. E-mail: warren.chan@utoronto.ca.
*Tel: +1 416 340-5230. E-mail: ian.mcgilvray@uhn.ca.

ORCID

Sonya A. MacParland: 0000-0002-8036-1425
Ian D. McGilvray: 0000-0003-4649-546X

Author Contributions

⬡S.A.M. and K.M.T. contributed equally and are co-first authors.

Notes

The authors declare no competing financial interest.

ACKNOWLEDGMENTS

We acknowledge the Canadian Institute of Health Research (Grant 136779 to I.D.M.) and Natural Sciences and Engineering Research Council for funding the project. K.M.T. thanks the NSERC Vanier Canada Graduate Scholarship Program and the Surgeon-Scientist Program at the University of Toronto for financial support. S.A.M. thanks the CASL/CIHR Hepatology Fellowship Program and the National CIHR Research Training Program in Hepatitis C for financial support. We would also like to acknowledge Doug Holmyard from the Mount Sinai Advanced Bioimaging Centre (Toronto, Canada), Dionne White from the Department of Immunology, University of Toronto (Toronto, Ontario), and Wilson Poon from the Institute of Biomaterials and Biomedical Engineering, University of Toronto (Toronto, Ontario).

REFERENCES

(1) Zhang, Y. N.; Poon, W.; Tavares, A. J.; McGilvray, I. D.; Chan, W. C. Nanoparticle-Liver Interactions: Cellular Uptake and Hepatobiliary Elimination. *J. Controlled Release* **2016**, *240*, 332−348.

(2) Wilhelm, S.; Tavares, A. J.; Dai, Q.; Ohta, S.; Audet, J.; Dvorak, H. F.; Chan, W. C. W. Analysis of Nanoparticle Delivery to Tumours. *Nat. Rev. Mater.* **2016**, *1*, 16014.

(3) Fischer, H. C.; Hauck, T. S.; Gomez-Aristizabal, A.; Chan, W. C. W. Exploring Primary Liver Macrophages for Studying Quantum Dot Interactions with Biological Systems. *Adv. Mater.* **2010**, *22*, 2520−2524.

(4) Murray, P. J.; Wynn, T. A. Protective and Pathogenic Functions of Macrophage Subsets. *Nat. Rev. Immunol.* **2011**, *11*, 723−737.

(5) Imamura, H.; Laberge, S.; Brault, A.; Cote, J.; Huet, P. M. Immunogenic Role of Kupffer Cells in A Rat Model of Acute Liver Allograft Rejection. *Liver Transplant.. Surg.* **1995**, *1*, 389−394.

(6) Bittmann, I.; Bottino, A.; Baretton, G. B.; Gerbes, A. L.; Zachoval, R.; Rau, H. G.; Lohrs, U. The Role of Graft-Resident Kupffer Cells and Lymphocytes of Donor Type During The Time Course After Liver Transplantation-A Clinico-Pathological Study. *Virchows Arch.* **2003**, *443*, 541−548.

(7) Lunov, f.; Syrovets, T.; Loos, C.; Beil, J.; Delacher, M.; Tron, K.; Nienhaus, G. U.; Musyanovych, A.; Mailander, V.; Landfester, K.; Simmet, T. Differential Uptake of Functionalized Polystyrene Nanoparticles by Human Macrophages and a Monocytic Cell Line. *ACS Nano* **2011**, *5*, 1657−1669.

(8) Kodali, V.; Littke, M. H.; Tilton, S. C.; Teeguarden, J. G.; Shi, L.; Frevert, C. W.; Wang, W.; Pounds, J. G.; Thrall, B. D. Dysregulation of Macrophage Activation Profiles by Engineered Nanoparticles. *ACS Nano* **2013**, *7*, 6997−7010.

(9) Mills, C. D.; Kincaid, K.; Alt, J. M.; Heilman, M. J.; Hill, A. M. M-1/M-2 Macrophages and the Th1/Th2 Paradigm. *J. Immunol.* **2000**, *164*, 6166−6173.

(10) Gordon, S.; Plueddemann, A.; Martinez Estrada, F. M.Macrophage Heterogeneity in Tissues: Phenotypic Diversity and Functions. *Immunol. Rev.* **2014**, *262*, 36−55.

(11) Qian, B.-Z.; Pollard, J. W. Macrophage Diversity Enhances Tumor Progression and Metastasis. *Cell* **2010**, *141*, 39−51.

(12) Peled, M.; Fisher, E. A. Dynamic Aspects of Macrophage Polarization During Atherosclerosis Progression and Regression. *Front. Immunol.* **2014**, *5*, 579 DOI: 10.3389/fimmu.2014.00579.

(13) Jones, S. W.; Roberts, R. A.; Robbins, G. R.; Perry, J. L.; Kai, M. P.; Chen, K.; Bo, T.; Napier, M. E.; Ting, J. P. Y.; DeSimone, J. M.; Bear, J. E. Nanoparticle Clearance Is Governed By Th1/Th2 Immunity and Strain Background. *J. Clin. Invest.* **2013**, *123*, 3061−3073.

(14) Mia, S.; Warnecke, A.; Zhang, X. M.; Malmstrom, V.; Harris, R. A. An optimized Protocol for Human M2Macrophages using M-CSF and IL-4/IL-10/TGF-beta Yields a Dominant Immunosuppressive Phenotype. *Scand. J. Immunol.* **2014**, *79*, 305−314.

(15) Rey-Giraud, F.; Hafner, M.; Ries, C. H. *In Vitro* Generation of Monocyte-Derived Macrophages under Serum-Free Conditions Improves Their Tumor Promoting Functions. *PLoS One* **2012**, *7*, e42656.

(16) Martinez, F. O.; Sica, A.; Mantovani, A.; Locati, M. Macrophage Activation and Polarization. *Front. Biosci., Landmark Ed.* **2008**, *13*, 453−461.

(17) Biswas, S. K.; Mantovani, A. Macrophage Plasticity and Interaction With Lymphocyte Subsets: Cancer As A Paradigm. *Nat. Immunol.* **2010**, *11*, 889−896.

(18) Murray, P. J.; Allen, J. E.; Biswas, S. K.; Fisher, E. A.; Gilroy, D. W.; Goerdt, S.; Gordon, S.; Hamilton, J. A.; Ivashkiv, L. B.; Lawrence, T.; Locati, M.; Mantovani, A.; Martinez, F. O.; Mege, J.-L.; Mosser, D. M.; Natoli, G.; Saeij, J. P.; Schultze, J. L.; Shirey, K. A.; Sica, A.; et al. Macrophage Activation and Polarization: Nomenclature and Experimental Guidelines. *Immunity* **2014**, *41*, 14−20.

(19) Herd, H. L.; Bartlett, K. T.; Gustafson, J. A.; McGill, L. D.; Ghandehari, H. Macrophage Silica Nanoparticle Response Is Phenotypically Dependent. *Biomaterials* **2015**, *53*, 574−582.

(20) Hoppstaedter, J.; Seif, M.; Dembek, A.; Cavelius, C.; Huwer, H.; Kraegeloh, A.; Kiemer, A. K. M2 Polarization Enhances Silica Nanoparticle Uptake By Macrophages. *Front. Pharmacol.* **2015**, *6*, 55 DOI: 10.3389/fphar.2015.00055.

(21) Etheridge, M. L.; Campbell, S. A.; Erdman, A. G.; Haynes, C. L.; Wolf, S. M.; McCullough, J. The Big Picture On Nanomedicine: The State of Investigational and Approved Nanomedicine Products. *Nanomedicine* **2013**, *9*, 1−14.

(22) Ambarus, C. A.; Krausz, S.; van Eijk, M.; Hamann, J.; Radstake, T. R. D. J.; Reedquist, K. A.; Tak, P. P.; Baeten, D. L. P. Systematic Validation of Specific Phenotypic Markers for *In Vitro* Polarized Human Macrophages. *J. Immunol. Methods* **2012**, *375*, 196−206.

(23) Metz, S.; Bonaterra, G.; Rudelius, M.; Settles, M.; Rummeny, E. J.; Daldrup-Link, H. E. Capacity of Human Monocytes to Phagocytose Approved Iron Oxide MR Contrast Agents In Vitro. *Eur. Radiol.* **2004**, *14*, 1851−1858.

(24) Raynal, I.; Prigent, P.; Peyramaure, S.; Najid, A.; Rebuzzi, C.; Corot, C. Macrophage Endocytosis of Superparamagnetic Iron Oxide Nanoparticles: Mechanisms and Comparison of Ferumoxides and Ferumoxtran-10. *Invest. Radiol.* **2004**, *39*, 56−63.

(25) Walkey, C. D.; Olsen, J. B.; Guo, H.; Emili, A.; Chan, W. C. W. Nanoparticle Size and Surface Chemistry Determine Serum Protein Adsorption and Macrophage Uptake. *J. Am. Chem. Soc.* **2012**, *134* (4), 2139−2147.

(26) Yu, M.; Chen, Z.; Guo, W.; Wang, J.; Feng, Y.; Kong, X.; Hong, Z. Specifically Targeted Delivery of Protein to Phagocytic Macrophages. *Int. J. Nanomed.* **2015**, *10*, 1743−1757.

(27) He, C.; Hu, Y.; Yin, L.; Tang, C.; Yin, C. Effects of Particle Size and Surface Charge On Cellular Uptake and Biodistribution of Polymeric Nanoparticles. *Biomaterials* **2010**, *31*, 3657−3666.

(28) Perrault, S. D.; Walkey, C.; Jennings, T.; Fischer, H. C.; Chan, W. C. Mediating Tumor Targeting Efficiency of Nanoparticles Through Design. *Nano Lett.* **2009**, *9*, 1909−1915.

(29) Hirn, S.; Semmler-Behnke, M.; Schleh, C.; Wenk, A.; Lipka, J.; Schaffler, M.; Takenaka, S.; Moller, W.; Schmid, G.; Simon, U.; et al.

DOI: 10.1021/acsnano.6b06245
ACS Nano 2017, 11, 2428−2443

Particle Size-Dependent and Surface Charge-Dependent Biodistribution of Gold Nanoparticles After Intravenous Administration. *Eur. J. Pharm. Biopharm.* **2011**, *77*, 407−416.
(30) Zhang, G.; Yang, Z.; Lu, W.; Zhang, R.; Huang, Q.; Tian, M.; Li, L.; Liang, D.; Li, C. Influence of Anchoring Ligands and Particle Size On The Colloidal Stability and *In Vivo* Biodistribution of Polyethylene Glycol-Coated Gold Nanoparticles in Tumor-Xenografted Mice. *Biomaterials* **2009**, *30*, 1928−1936.
(31) Annenkov, A. Y.; Baranova, F. S. Lipopolysaccharide-Dependent and Lipopolysaccharide-Independent Pathways of Monocyte Desensitisation to Lipopolysaccharides. *J. Leuk. Biol.* **1991**, *50*, 215−222.
(32) Granowitz, E. V.; Porat, R.; Mier, J. W.; Orencole, S. F.; Kaplanski, G.; Lynch, E. A.; Ye, K.; Vannier, E.; Wolff, S. M.; Dinarello, C. A. Intravenous Endotoxin Suppresses The Cytokine Response of Peripheral-Blood Mononuclear-Cells of Healthy Humans. *J. Immunol.* **1993**, *151*, 1637−1645.
(33) Rogy, M. A.; Oldenburg, H. S. A.; Coyle, S.; Trousdale, R.; Moldawer, L. L.; Lowry, S. F. Correlation Between Acute Physiology and Chronic Health Evaluation (APACHE) II Score and Immunological Parameters in Critically Ill Patients With Sepsis. *Br. J. Surg.* **1996**, *83*, 396−400.
(34) Kolios, G.; Valatas, V.; Kouroumalis, E. Role of Kupffer Cells in The Pathogenesis of Liver Disease. *World J. Gastroenterol.* **2006**, *12*, 7413−7420.
(35) Tsoi, K. M.; MacParland, S. A.; Ma, X.-Z.; Spetzler, V. N.; Echeverri, J.; Ouyang, B.; Fadel, S. M.; Sykes, E. A.; Goldaracena, N.; Kaths, J. M.; Conneely, J. B.; Alman, B. A.; Selzner, M.; Ostrowski, M. A.; Adeyi, O. A.; Zilman, A.; McGilvray, I. D.; Chan, W. C. W. Mechanism of Hard-Nanomaterial Clearance By The Liver. *Nat. Mater.* **2016**, *15*, 1212−1221.
(36) Lavin, Y.; Winter, D.; Blecher-Gonen, R.; David, E.; Keren-Shaul, H.; Merad, M.; Jung, S.; Amit, I. Tissue-Resident Macrophage Enhancer Landscapes Are Shaped by the Local Microenvironment. *Cell* **2014**, *159*, 1312−1326.
(37) Gautier, E. L.; Shay, T.; Miller, J.; Greter, M.; Jakubzick, C.; Ivanov, S.; Helft, J.; Chow, A.; Elpek, K. G.; Gordonov, S.; et al. Gene-Expression Profiles and Transcriptional Regulatory Pathways That Underlie The Identity and Diversity of Mouse Tissue Macrophages. *Nat. Immunol.* **2012**, *13*, 1118−1128.
(38) Bilzer, M.; Roggel, F.; Gerbes, A. L. Role of Kupffer Cells in Host Defense and Liver Disease. *Liver Int.* **2006**, *26*, 1175−1186.
(39) Frens, G. Controlled Nucleation for Regulation of Particle-Size in Monodisperse Gold Suspensions. *Nature, Phys. Sci.* **1973**, *241*, 20−22.
(40) Perrault, S. D.; Chan, W. C. W. Synthesis and Surface Modification of Highly Monodispersed, Spherical Gold Nanoparticles of 50−200 nm. *J. Am. Chem. Soc.* **2009**, *131*, 17042−17043.
(41) Albanese, A.; Tsoi, K. M.; Chan, W. C. W. Simultaneous Quantification of Cells and Nanomaterials by Inductive-Coupled Plasma Techniques. *Jala* **2013**, *18*, 99−104.
(42) Lee, S. M.; Schelcher, C.; Demmel, M.; Hauner, M.; Thasler, W. E. Isolation of Human Hepatocytes By a Two-Step Collagenase Perfusion Procedure. *J. Visualized Exp.* **2013**, *79*, 50615 DOI: 10.3791/50615.
(43) Mahnke, Y. D.; Roederer, M. Optimizing a Multicolor Immunophenotyping Assay. *Clin. Lab. Med.* **2007**, *27*, 469−85.

DOI: 10.1021/acsnano.6b06245
ACS Nano 2017, 11, 2428−2443